HHS Public Access

Author manuscript

Gastroenterology. Author manuscript; available in PMC 2023 July 10.

Published in final edited form as:

Gastroenterology. 2023 July ; 165(1): 133–148.e17. doi:10.1053/j.gastro.2023.02.049.

A TEAD2-driven endothelial-like program shapes basal-like differentiation and metastasis of pancreatic cancer

Hye-Been Yoo[1], **Jin Woo Moon**[2], **Hwa-Ryeon Kim**[1], **Hee Seung Lee**[3], **Koji Miyabayashi**[4], **Chan Hee Park**[3], **Sabrina Ge**[5,6], **Amy Zhang**[5,7], **Yoo Keung Tae**[3], **Yujin Sub**[8], **Hyun-Woo Park**[1], **Heon Yung Gee**[8], **Faiyaz Notta**[5,6,7], **David A. Tuveson**[9], **Seungmin Bang**[3], **Mi-Young Kim**[2,10], **Jae-Seok Roe**[1,10]

[1]Department of Biochemistry, Yonsei University, Seoul, Korea

[2]Department of Biological Sciences, Korea Advanced Institute of Science and Technology, Daejeon, Korea

[3]Division of Gastroenterology, Department of Internal Medicine, Yonsei University College of Medicine, Seoul, Korea

[4]Department of Gastroenterology, Graduate School of Medicine, The University of Tokyo, Tokyo, Japan

[5]Princess Margaret Cancer Centre, Toronto, Ontario, Canada

[6]Department of Medical Biophysics, University of Toronto, Toronto, Ontario, Canada

[7]PanCuRx Translational Research Initiative, Ontario Institute for Cancer Research, Toronto, Ontario, Canada

[8]Department of Pharmacology, Brain Korea 21 PLUS Project for Medical Sciences, Yonsei University College of Medicine, Seoul, Korea

[9]Lustgarten Foundation Dedicated Laboratory at Cold Spring Harbor Laboratory, Cold Spring Harbor, New York, USA

Abstract

[10]Corresponding authors: **Jae-Seok Roe:** Department of Biochemistry, College of Life Science and Biotechnology, Yonsei University, Seoul, Korea (jroe@yonsei.ac.kr); **Mi-Young Kim**: Department of Biological Sciences, Korea Advanced Institute of Science and Technology, Daejeon, Korea (miyoungkim@kaist.ac.kr).

AUTHOR CONTRIBUTION

Conceptualization: Jae-Seok Roe, Hwa-Ryeon Kim, Hye-Been Yoo

Study design: Jae-Seok Roe, Mi-Young Kim, Hwa-Ryeon Kim, Hye-Been Yoo, Jin Woo Moon

Data acquisition: Hye-Been Yoo, Jin Woo Moon, Hwa-Ryeon Kim, Hee Seung Lee, Koji Miyabayashi, Chan Hee Park, Yoo Keung Tae

Analysis and interpretation of data: Sabrina Ge, Amy Zhang, Faiyaz Notta, David A. Tuveson

Drafting of the original manuscript: Jae-Seok Roe, Mi-Young Kim, Hwa-Ryeon Kim, Hye-Been Yoo, Jin Woo Moon

Drafting of the revised manuscript: Jae-Seok Roe, Hwa-Ryeon Kim, Hye-Been Yoo

Technical, or material support: Seungmin Bang, Heon Yung Gee, Yujin Sub, Hyun-Woo Park,

Study supervision: Jae-Seok Roe, Mi-Young Kim

[#]Author names in bold designate shared co-first authorship

DISCLOSURES

The authors disclose no conflicts.

BACKGROUND AND AIMS—Pancreatic ductal adenocarcinoma (PDA), with its highly metastatic propensity, is one of the most lethal subtypes of pancreatic cancer. Although recent large-scale transcriptomic studies have demonstrated that heterogeneous gene expressions play an essential role in determining molecular phenotypes of PDA, biological cues for and consequences of distinct transcriptional programs remain unclear.

METHODS—We developed an experimental model that enforces the transition of PDA cells toward a basal-like subtype. We combined epigenome and transcriptome analyses with extensive *in vitro* and *in vivo* evaluations of tumorigenicity to demonstrate the validity of basal-like subtype differentiation in association with endothelial-like enhancer landscapes via TEAD2. Finally, we used loss-of-function experiments to investigate the importance of TEAD2 in regulating reprogrammed enhancer landscape and metastasis in basal-like PDA cells.

RESULTS—Aggressive characteristics of the basal-like subtype are faithfully recapitulated *in vitro* and *in vivo*, demonstrating the physiological relevance of our model. Further, we showed that basal-like subtype PDA cells acquire a TEAD2-dependent pro-angiogenic enhancer landscape. Genetic and pharmacological inhibitions of TEAD2 in basal-like subtype PDA cells impair their pro-angiogenic phenotypes *in vitro* and cancer progression *in vivo*. Lastly, we identify CD109 as a critical TEAD2 downstream mediator that maintains constitutively activated JAK-STAT signaling in basal-like PDA cells and tumors.

CONCLUSIONS—Our findings implicate a TEAD2-CD109-JAK/STAT axis in the basal-like differentiated pancreatic cancer cells and as a potential therapeutic vulnerability.

Keywords

Pancreatic cancer; Molecular subtype; Enhancer reprogramming

INTRODUCTION

Initiation and progression of pancreatic ductal adenocarcinoma (PDA) require recurrent genomic changes[1]. In contrast, there are extensive intra- and inter-tumor heterogeneities in the PDA transcriptome. Such transcriptional diversity allows stratifying PDA into two or more major molecular subtypes[2–5], which have different morphologic features, prognoses, and responses to chemotherapy, indicating pathophysiologic relevance of the molecular subtype classification[2, 4, 6]. Currently there is no effective PDA therapeutic targeting aberrant genomic alterations. Finding relevant changes of molecular profiles beyond simple genetic mutations may help to define subtype classification of PDA and discover potential targets for PDA treatment.

Functional acquisition or loss of transcriptional regulators has been shown to play a decisive role in determining molecular subtypes of PDA. For example, increased expressions of transcription factors (TFs), represented by the ΔN isoform of TP63, are critical for driving and maintaining the basal-like subtype identity of PDA cells[2, 7, 8] whereas decreased expressions of HNF4A and GATA4/6, hallmarks of the classical subtype, are associated with basal-like PDA[9, 10]. However, heterogeneous expression patterns of TP63 and its targets have been observed in basal-like patient-derived PDA organoids[11], indicating that a subset of basal-like PDA tumors may not require TP63-dependent transcriptional programs. Loss-

of-function mutations in chromatin-modifying enzymes, including KDM6A, are examples of chromatin changes contributing to the determination of the basal-like subtype in PDA[2, 12]. The epigenetic regulation is considered to cooperate with, rather than independent from, genomic changes in specifying the molecular phenotype of PDA, exemplified by the amplification of the mutant *KRAS* allele leading to an allelic imbalance in basal-like subtype PDA[5]. Nonetheless, suitable experimental model that can explore cause-effect relationships for subtype specification is not provided yet.

An important question in PDA is whether their molecular subtypes can be reprogrammed as the ability to reprogram PDA subtypes may help to develop subtype-specific treatments. Supporting this possibility, overexpression of DNp63 or GLI2 can lead to progenitor-to-squamous subtype switch in human PDA cells whereas depletion of these TFs impairs the squamous identity of PDA[7, 8]. Notably, the loss of CXCR2 results in a transition from the squamous subtype to other subtypes, suggesting fluctuations in paracrine signaling in the tumor microenvironment (TME) are likely to influence the maintenance of molecular subtypes[13]. Patient-derived PDA organoids transplanted into the duct and into the interstitial space of the pancreas tend to form tumors with different molecular subtypes, suggesting that the tissue microenvironment is essential in determining molecular subtypes[11]. Supporting this is the demonstration that culture condition contributes to the molecular subtype of *ex vivo* PDA organoid[14]. Therefore, the existence of distinct epigenetic alterations that accommodate microenvironmental change is strongly anticipated.

The unique pattern of TME of PDA is likely to contribute to molecular subtypes determination and cancer progression. Local tumor progression has been proposed to occur through repeated cycles of dissemination and self-seeding at the site where the primary cancer initially occurs[15]. With the notion that the basal-like subtype is superior to other subtypes in primary tumor growth and metastasis, we hypothesize that such “dissemination-seeding cycle” is an environmental cue for a gradual shift toward the most aggressive form of PDA, the basal-like subtype[2–4]. We further hypothesize that the molecular changes occurred during the “dissemination-seeding cycle” can be mimicked, at least in part, by “cell detachment and re-attachment” in culture thereby driving a shift to more aggressive molecular subtype. Our goal, through developing these platforms, is to identify key epigenetic modulations responsible for the adaptation and evolution of PDA to drastic surrounding extracellular environment changes.

MATERIALS AND METHODS

See the Supplementary Methods for descriptions of description of the methods, reagents, and statistics.

RESULTS

Establish an *in vitro* subtype switching model that recapitulates basal-like transcriptional phenotypes of PDA

To test our hypothesis, we cultured cancer cells that typically grow in monolayer (Parental; hereafter referred to as Par) on ultra-low attachment plates to render anchorage-independent

growth for about two weeks and subsequently re-adapted surviving cells to the monolayer culture for propagation (Spheroid-derived; hereafter referred to as Sph) (Figure 1A). We established Par-Sph pairs using *Kras*$^{G12D/+}$;*Trp53*$^{R172H/+}$;*Pdx1-Cre* (KPC) mouse cell lines (FC1199-Par/FC1199-Sph and NB490-Par/NB490-Sph) and a well-documented classical subtype human PDA cell line, SUIT2 (SUIT2-Par/SUIT2-Sph). Most spontaneous pancreatic tumors grown in KPC mice exhibit relatively well-differentiated morphology[16], similar to morphological properties of the classical molecular subtype. When Par-Sph pairs were propagated in the monolayer condition, there was no noticeable differences in their morphologies or proliferation rates (Figure 1B and 1C; Supplementary Figure S1A and S1B). In contrast, Sph cells had increased abilities to form spheroids under ultra-low attachment conditions (Figure 1D; Supplementary Figure S1C) and colonies in soft agar (Figure 1E; Supplementary Figure S1D) than Par cells. Sph cells also had higher transwell migration and matrigel invasion capabilities (Supplementary Figure S1E and S1F).

We hypothesized that transcriptional differences between Par and Sph cells regulated their phenotypic differences when grown under ultra-low attachment conditions. To identify differentially expressed genes, we conducted RNA sequencing (RNA-seq) analysis of these cells grown in a monolayer. We first confirmed their different mRNA expression patterns (Supplementary Figure S1G) then employed an unbiased gene set enrichment analysis (GSEA) to compare their transcriptome profiles. Top-ranked signatures enriched in Sph cell were primarily grouped into extracellular matrix, KRAS signaling, and vasculature development (Figure 1F). Notably, epithelial-to-mesenchymal transition (EMT) and the hyperactivation of mutant KRAS signaling were known molecular features of the basal-like subtype PDA[5, 17], whereas the importance of vasculature development in basal-like subtype was unknown. To further determine if the Par-to-Sph transition resembled classical-to-basal-like molecular subtype switch, we found from GSEA that the squamous/basal-like gene signatures were positively enriched whereas the progenitor/classical gene signatures were negatively enriched in Sph cells (Figure 1G; Supplementary Figure S1H). GSEA of KRAS downstream targets identified an increase of KRAS ON and a decrease of KRAS OFF signatures in Sph cells (Figure 1H), although differences in KRAS expression or ERK phosphorylation were negligible (Supplementary Figure S1I). Finally, we confirmed that gene sets related to blood vessel development were significantly enriched in Sph cells (Figure 1I; Supplementary Figure S1J). To check if the anchorage-independent culture condition selectively enriched the basal-like subtype cells that were present in the monolayer culture, RNA-seq analysis of spheroid cultured cells, the intermediate stage of Par and Sph, was conducted. The basal-like gene expression did not increase in the spheroid cultured cells (Supplementary Figure S1K). Intriguingly, we found that the expression of classical subtype genes significantly increased in spheroid cultured cells then reduced in Sph cells (Supplementary Figure S1K and S1L). These results implicated that the adaptation process of cell detachment and re-attachment proactively reprogramed rather than selected the molecular subtype. Moreover, we did not identify an increased expression of DNp63 or its downstream targets in FC1199-derived Sph cells (Supplementary Figure S1M). Our results suggest that transcriptional alterations imposed through manipulating anchorage independent growth reprograms PDA cells to basal-like subtype in a DNp63-independent manner.

Introducing basal-like subtype promotes primary tumor growth and metastasis

To examine if characteristics of the basal-like subtype observed *in vitro* were preserved *in vivo*, we subcutaneously injected FC1199-Par and -Sph cells into flanks of syngeneic mice and found that tumors derived from Sph cells grew faster than those derived from Par cells (Figure 2A). Mice bearing Sph-tumors exhibited significantly increased lung metastases (Figure 2B) and survived shorter (an average of 65 days vs. 123 days) than mice bearing Par-tumors (Figure 2C). To check the validity of these findings in the human PDA setting, we injected SUIT2-Par and -Sph cells subcutaneously into immunocompromised mice and found similarly that SUIT2-Sph cells formed faster growing primary tumor and more metastatic lung colonization (Supplementary Figure S2A–S2B).

RNA-seq analysis of freshly isolated cancer cells from tumors followed by GSEA verified the conservation of the transcriptional signatures of the basal-like PDA identity of FC1199-Sph-derived tumors *in vivo* (Figure 2D). The previously observed activation of the KRAS pathway and vasculature development transcriptional phenotypes were also enriched in Sph-derived tumors than in Par-derived tumors (Supplementary Figure S2C and S2D).

In order to better reflect PDA progression in patients, we orthotopically transplanted cells in the pancreas and observed that implanted FC1199-Sph cells formed larger primary tumors than FC1199-Par cells (Figure 2E). The degree that PDA cells colonized in the liver and the lung, two major organs where PDA cells metastasize to[18], was also significantly higher in mice transplanted with FC1199-Sph cells than with FC1199-Par (Figure 2F and 2G; Supplementary Figure S2E). Similar results were observed from orthotopic xenograft experiments using SUIT2-Par and SUIT2-Sph cells (Figure 2H and 2I). To evaluate the biological relevance of basal-like programs in the tumor, we conducted immunohistochemistry (IHC) analyses and found increased CD34-positive microvessels in the tumor stroma and decreased classical marker HNF4A-positive cells in Sph-derived tumors (Figure 2J and Supplementary Figure S2F). Further, IHC of COL6A1 (Collagen Type VI Alpha 1 Chain) and Masson's trichrome staining indicated the deposition of extracellular matrix (ECM) proteins in Sph-derived tumors (Figure 2K and 2L). These findings indicated that our approach faithfully recapitulated basal-like properties of PDA cells, allowing us to explore molecular mechanisms of subtype switching.

Basal-like subtype conversion is associated with an endothelial-like transcriptional enhancer landscape

To explore the association between subtype difference and chromatin changes, we mapped the distribution of H3K4me1, H3K27ac, and H3K4me3 by using chromatin immunoprecipitation and sequencing (ChIP-seq) and chromatin accessibility by using Assay for Transposase-Accessible Chromatin using sequencing (ATAC-seq) (Supplementary Figure S3A). H3K4me1 and H3K27ac are reliable markers for enhancer identity and activity, respectively, and H3K4me3 is located exclusively at promoters. While there was no apparent difference in global levels of histone modifications (Supplementary Figure S3B), we identified hundreds of genomic regions with > 4-fold differences in H3K27ac between FC1199-Par cells and FC1199-Sph cells. Hereafter, we refer regions that gain or lose H3K27ac signals in FC1199-Sph cells as *GAIN-S* (n = 700) and *LOSS-S* (n = 334),

respectively (Supplementary Figure S3C). More than 85% of *GAIN-S* and *LOSS-S* regions lie outside of transcription start site, suggesting that they represent enhancer elements. Although chromatin accessibility showed no marked difference between FC1199-Par and FC1199-Sph cells, the pattern of H3K4me1 accumulation in FC1199-Sph cells was similar to that of H3K27ac, indicating a "poised" state of accessibility in these enhancers (Figure 3A and 3B; Supplementary Figure S3D and S3E).

Next, we performed the GREAT tool-based unbiased ontology analysis of genes located around *GAIN-S* sites (*GAIN-S* genes) and *LOSS-S* sites (*LOSS-S* genes)[19]. We found that eight of the top 10 enriched GO terms of *GAIN-S* genes were closely related to vasculature development, with the strongest term being "angiogenesis" (Figure 3C). Indeed, vasculature development was among the top-ranked signatures enriched in Sph cells (Figure 1F). *LOSS-S* genes were only associated with the GO term "magnesium ion binding" (Supplementary Figure S3F). Furthermore, we found a significant association of enhancer activity and gene expression from GSEA of RNA-seq data (Figure 3D; Supplementary Figure S3G). In support of this, we found increased expression of genes related to angiogenesis, such as *CXCL12*, *CD109*, and *CCL2*, located in close proximity to *GAIN-S* enhancers in basal-like subtype PDA cells from mouse and human (Figure 3E; Supplementary Figure S3H). Moreover, GSEA showed that the expression of *GAIN-S* genes was elevated in the basal-like subtype compared to the classical subtype in PDA from patients and in patient-derived PDA organoids (Figure 3F). Conversely, the expression of *LOSS-S* genes was downregulated in both basal-like PDA cells and basal-like subtype PDA from patients (Supplementary Figure S3I–K).

We hypothesized that basal-like subtype reprogramming endowed PDA cells to acquire behavioral patterns of endothelial cells, which might assist to enhance aggressiveness, and checked whether Sph cells could facilitate experimental blood vessel formation. First, we performed tube formation and transwell migration assays using human umbilical vein endothelial cells (HUVECs) in the presence of conditioned media (CM) from FC1199-Par and -Sph cells. Compared to FC1199-Par CM, FC1199-Sph CM increased the capability of HUVECs in forming tubes on matrigel and passing through a transwell membrane (Figure 3G). Of note, a large number of *GAIN-S* genes encode secreted proteins, suggesting that basal-like subtype PDA cells acquire pro-angiogenic secretory phenotype through activated *GAIN-S* enhancer programs. It has been proposed that some cancer cells can form microvascular-like channels, termed "vascular mimicry (VM)", that can drive a sub-population of breast cancer cells to metastasize to distant sites[20]. To our surprise, compared to FC1199-Par or NB490-Par cells, FC1199-Sph or NB490-Sph cells formed robust tubular structures when grown on matrigel, a well-established phenotype of cell-autonomous VM (Figure 3H; Supplementary Figure S3L). Moreover, applying FC1199-Sph CM or NB490-Sph CM to FC1199-Par or NB490-Par cells was sufficient to facilitate vessel-like tube formation (Figure 3H; Supplementary Figure S3L), suggesting cell non-autonomous mechanism of VM.

Tumor endothelial enhancer activation in basal-like subtype PDA requires TEAD2 activity

A prior work shows that upregulated DNp63 or GLI2 is responsible for reprogramming the enhancer landscape of the squamous subtype[7, 8], but neither *Tp63* nor *Gli2* mRNA expression was detected in FC1199-Par or -Sph cells (Supplementary Figure S1M and S4A). These data led us to identify TFs that activated *GAIN-S* enhancers. To evaluate TF motif enrichment, genomic regions extending 500 bp upstream and downstream from the center of each *GAIN-S* enhancer peaks were analyzed through the HOMER *de novo* motif discovery tool (Figure 4A). Among top enriched motifs at *GAIN-S* regions, we decided to focus on the Hippo pathway TF TEAD2 because TEAD2 had the largest increase in expression in FC1199-Sph compared to FC1199-Par (Figure 4B) and was the second-highest expressed gene (Supplementary Figure S4B) in our RNA-seq analysis. The TEAD2 motif was not discovered when analyzing *LOSS-S* enhancers (Supplementary Figure S4C). Consistent with the results from basal-like subtype switch in FC1199 cells, the *TEAD2* mRNA expression was significantly upregulated in PDA from patients and PDA cell lines with the basal-like subtype, including basal-like subtype PDA cells lacking *TP63* mRNA expression (Figure 4C; Supplementary Figure S4D). We then mapped genome-wide enrichment of TEAD2 using FC1199 cells expressing exogenous Flag-tagged TEAD2, because of high homologies among TEAD1–TEAD4. We identified that TEAD-related motifs were strongly enriched at Flag-TEAD2 peaks (Supplementary Figure S4E) and observed that the occupancy of Flag-TEAD2 was stronger at the center of *GAIN-S* regions than *LOSS-S* regions, supporting the preferential regulation of TEAD2 (Figure 4D).

Next, we evaluated whether increased TEAD2 expression was necessary for maintaining *GAIN-S* enhancer activity and its associated transcriptional programs of endothelial cell lineage. We found that both TEAD2 short hairpin RNAs (shRNAs) and verteporfin, an inhibitor of the interaction of YAP with the TEAD family[21], reduced H3K27ac occupancy to a similar degree at the *GAIN-S* region, but not randomly selected sites, in FC1199-Sph cells (Figure 4E and 4F; Supplementary Figure S4F and S4G). Accordingly, RNA-seq analysis revealed downregulation of *GAIN-S* genes in TEAD2-deficient FC1199-Sph cells (Figure 4G). Among GO terms associated with most downregulated genes by TEAD2 shRNA were several related to endothelial cell development (Supplementary Figure S4H), indicating that a major function of TEAD2 in basal-like PDA cells was maintaining the feature of endothelial lineage program.

We defined downstream targets of TEAD2 as core targets of TEAD2 that had increased H3K27ac occupancy and downregulated expression in FC1199-Sph cells upon TEAD2 knockdown and, as a result, identified a total of 70 genes (Supplementary Figure S4I), including *Ccl2*, *Cxcl12*, and *Cd109* (Supplementary Figure S4J). To determine the relevance of these genes in molecular subtypes of human PDAs, we used single sample GSEA (ssGSEA) to calculate the arbitrary expression score and found that PDAs in the PanCuRx dataset[22] classified as the basal-like subtype expressed a higher level of TEAD2 targets than those of the classical subtype (Figure 4H). Conversely, PDAs expressing higher levels of TEAD2 targets were more likely to be the basal-like subtype (Figure 4I; Supplementary Figure S4K). Importantly, patients whose PDAs expressed higher TEAD2 targets had a worse prognosis (Figure 4J). Consistently, the expression of TEAD2 core targets was higher

in the basal-like subtype cluster than in the classical subtype cluster in a scRNA-seq dataset of 15 PDAs[5] (Figure 4K). Mutant *KRAS* copy number aberrations is an emerging hallmark of the basal-like subtype PDAs[5, 23]. We therefore examined whether the level of TEAD2 expression was related to the mutation status of *KRAS* in PDAs and found that those with high TEAD2 expression were enriched for major allelic imbalance of mutant *KRAS* than TEAD2-low tumors (Supplementary Figure S4L and S4M). Moreover, TEAD2 deficiency suppressed the transcription of KRAS targets (Supplementary Figure S4N).

Suppression of TEAD2 attenuates tumor progression and increases chemotherapy response of basal-like PDA

We then examined functional consequences of TEAD2 depletion *in vitro* and *in vivo*. Knockdown of TEAD2 in Sph cells using shRNAs suppressed mRNA levels of *TEAD2* and its core targets (Supplementary Figure S5A and S5B) and impaired transwell migration and matrigel invasion capabilities (Figure 5A and 5B), but did not change cell proliferation or oncosphere formation (Supplementary Figure S5C and S5D). Furthermore, CM obtained from TEAD2-depleted cells had significantly reduced ability in recruiting HUVECs (Figure 5C) and inhibiting TEAD2 by either shRNAs or verteporfin reduced the ability of PDA Sph cells to form vasculature-like networks (Figure 5D; Supplementary Figure S5E and S5F).

To extend our findings into *in vivo* settings, we transplanted the TEAD2-depleted or control FC1199-Sph cells subcutaneously into syngeneic mice. We found that FC1199-Sph cells expressing either TEAD2 shRNA formed slower growing tumors and colonized less at the lung than their control counterparts (Figure 5E and 5F). Similar results were observed from orthotopic transplantation experiments using TEAD2 shRNA-expressing FC1199-Sph and SUIT2-Sph cells (Figure 5G–5I; Supplementary Figure S5G). Notably, compared to controls, orthotopic Sph TEAD2 shRNA tumors had reduced CD34-positive microvessels and COL6A1 expression while having increased HNF4A-positive cells (Figure 5J; Supplementary Figure S5H and S5I). Consistently, overexpressing a well-documented TEAD2-dominant negative (DN) mutant[21] in FC1199-Sph cells reduced primary tumor growth and lung metastatic lesions (Supplementary Figure S5J and S5K).

Different molecular subtypes of PDA respond to chemotherapy differently, with the basal-like subtype having the least sensitivity[6]. Because the TEAD2 deficiency impaired the basal-like identity of PDA cells, we examined if TEAD2 inhibition altered the responses to chemotherapy *in vivo* using a low-dose (25mg/kg body weight twice weekly) instead of the standard dose (50–100mg/kg body weight twice weekly) gemcitabine. We found that a combination of verteporfin with gemcitabine significantly suppressed the growth of subcutaneous tumors derived from Sph cells whereas neither gemcitabine nor verteporfin alone did (Figure 5K). These findings suggest that TEAD2 is critical to maintain basal-like identity and aggressiveness of PDA cells, including the insensitivity to chemotherapy, *in vivo*.

TEAD2-dependent CD109 upregulation regulates the activation of STAT3 and tumor progression

CD109, a glycosylphosphatidylinositol (GPI) anchored cell surface protein and is secreted from cultured cancer cells[24, 25], has been shown to regulate Janus kinase (JAK)-dependent signal transducer and activator of transcription 3 (STAT3) activation in metastatic lung adenocarcinoma cells[26]. Since the gene encoding CD109 was among 70 TEAD core targets, we determined if CD109 was a critical effector of the TEAD2 pathway in potentiating the JAK-STAT3 pathway in the basal-like PDA cells (Figure 6A). First, we confirmed the enrichment of STAT3 signatures in human PDAs and FC1199-Sph cells. (Figure 6B and 6C; Supplementary Figure S6A–S6C). Depletion of TEAD2 expression downregulated both CD109 expression and phosphorylated STAT3 (pSTAT3) in FC1199-Sph cells (Figure 6D). Further, compared to FC1199-Par cells, FC1199-Sph cells displayed higher levels of phosphorylated STAT3 (pSTAT3), which was reduced by the treatment of pyridone 6 (P6), a pan-Jak-kinase inhibitor (Figure 6E).

Although interleukin-6 (IL-6) family cytokines are major ligands for activating the kinase activity of JAK[27], they were not upregulated in FC1199-Sph cells whereas CD109 did (Supplementary Figure S6D). Therefore, we examined if CD109 was critical in maintaining STAT3 signaling. We compared RNA-seq data of FC1199-Sph cells expressing CD109 shRNAs vs. STAT3 shRNAs and found that gene expression profiles of CD109-depleted cells and of STAT3-depleted cells were highly similar (Figure 6F; Supplementary Figure S6E and S6F). Accordingly, the top 200 downregulated genes upon STAT3 depletion were suppressed upon CD109 depletion (Figure 6G; Supplementary Figure S6G). The STAT3 signatures obtained from human PDAs or from STAT3 knockdown in FC1199-Sph cells were positively enriched in FC1199-Sph cells, which were compromised by verteporfin treatment or TEAD2 shRNAs expression (Supplementary Figure S6H and S6I). Furthermore, both depleting CD109 and depleting STAT3 abolished the vasculature-like network forming ability of FC1199-Sph cells (Figure 6H and 6I). These results supported our model that CD109 upregulation drove the activation of the JAK-STAT3 pathway in the basal-like subtype PDA cells.

We then determined whether the kinase activity of JAK is required for tumor growth, as multiple kinases could phosphorylate STAT3[28, 29]. P6 treatment of mice transplanted with FC1199-Par or FC1199-Sph cells did not reduce body weight but reduced numbers of pSTAT3-positive cells in tumors (Figure 6J and 6K; Supplementary Figure S6J) and significantly reduced primary tumor growth and metastatic colonization to liver and lung of FC1199-Sph-derived tumors (Figure 6L–6N). We next examined the functional importance of CD109 upregulation in PDA *in vivo*. Our analysis of publicly available datasets revealed that while the CD109 expression was not detected in the normal human pancreas, CD109 expression was detected in multiple human cancer types, including PDA (Supplementary Figure S6K and S6L). Further, we found that orthotopic primary tumors of FC1199-Sph cells expressing CD109 shRNA grew slower than their control counterparts (Figure 6O). Strikingly, CD109 depletion substantially retarded metastatic colonization in the lung and, to a lesser degree, in the liver (Figure 6P and 6Q). Concordantly, higher expression of CD109 in PDA correlated with shorter median overall survival of PDA patients (Figure 6R).

CD109 upregulation predisposes characteristics of the basal-like subtype in human PDA

To evaluate the human relevance of our findings, we separated ten human PDA cell lines into two groups (CD109^{high} and CD109^{low}) based on western blot analysis of their intracellular and secreted CD109, and compared to the pair of FC1199-Sph and FC1199-Par cells (Figure 7A; Supplementary Figure S7A). Consistently, the mRNA expression of *TEAD2* was significantly higher in CD109^{high} cells than in CD109^{low} cells (Supplementary Figure S7B). Furthermore, similar to FC1199-Sph, CD109^{high} cells exhibited higher levels of pSTAT3 than CD109^{low} cells (Figure 7A). CD109 potentiates the epidermal growth factor receptor (EGFR)-mediated phosphorylation of protein kinase B (also known as AKT)[30], and phosphorylation of AKT was high in four of five CD109^{high} cell lines (Figure 7A). Neither ERK phosphorylation nor KRAS expression was different between CD109^{high} and CD109^{low} cells (Figure 7A). Expressions of known classical markers (HNF4A or GATA6) were, to a varying degree, enriched in CD109^{low} cells (Figure 7A; Supplementary Figure S7C) whereas expressions of known basal-like subtype markers (TP63, KRT5/6A, and S100A2) were restricted to a subset of CD109^{high} cells (Figure 7A; Supplementary Figure S7D). There was no correlation between expression patterns of CD109 and well-established EMT markers (ZEB1, VIM, N-Cad, and E-Cad) or cell proliferation (Figure 7A; Supplementary Figure S7E, S7F). However, CD109^{high} cells had higher capabilities of matrigel invasion and vascular mimicry (Figure 7B; Supplementary Figure S7G–S7H).

To determine the transcriptional activity of STAT3 in CD109^{high} and CD109^{low} cells, we examined the genomic distribution of H3K27ac via ChIP-seq analysis. We found more than two-fold of H3K27ac occupancy at known STAT3-binding sites in CD109^{high} cells than in CD109^{low} cells (Figure 7C; Supplementary Figure 7I), but negligible differences of the H3K27ac signal at H3K27ac-enriched regions (Supplementary Figure S7J). The positive enrichment of STAT3 target gene signatures in CD109^{high} cells further supported STAT3-mediated transcriptional activation (Supplementary Figure S7K). In support of these results, GSEA revealed a positive enrichment of the basal-like gene signature in CD109^{high} cells, whereas the classical gene signature was enriched in CD109^{low} cells (Figure 7D). The top 200 downregulated genes upon TEAD2 or CD109 depletion in FC1199-Sph were associated with CD109^{high} cells (Supplementary Figure S7L). The functional role and human relevance of TEAD2 was further supported by GSEA showing the depletion of gene signatures of TEAD2 core target or squamous identity in verteporfin-treated KP4 cells (Figure 7E).

A recent study has identified an association between morphological patterns and molecular subtypes[31]. For example, PDAs with more than 50% of ‘non-gland forming’ components were related to the basal-like subtype. We therefore examined if the degree of CD109 expression was associated with non-gland forming patterns in pathologically confirmed human PDAs. We assessed CD109 in a total of 92 surgically resected PDA specimens with IHC and, based on the CD109 staining intensities, divided them into CD109^{weak} (n = 36), CD109^{moderate} (n = 37), and CD109^{strong} (n = 19) groups (Figure 7F). We sought to determine if the CD109 staining intensity was associated with the morphological subtype and found that the proportion of the non-glandular component was significantly higher in CD109^{strong} PDAs than in CD109^{weak} and CD109^{moderate} PDAs (Figure 7G). In accordance with known features of the basal-like subtype, patients with CD109^{strong} PDAs displayed

higher probability of tumor relapse and shorter overall survival than others (Figure 7H and 7I).

DISCUSSION

Here, we establish a reliable approach that installs known molecular characteristics of basal-like subtype in mouse and human PDA cells. Our results suggest that transcriptional alterations imposed by manipulating anchorage-independent growth reprograms PDA cells to basal-like subtype in a DNp63-independent manner. Further, our efforts to profile PDA epigenome have identified tumor endothelial-like enhancers maintained by TEAD2 as a key component of the identity in basal-like PDA cells. Importantly, through comprehensive *in vitro* and *in vivo* characterizations of models of different subtypes of PDA, we implicate that pro-angiogenic enhancers render increased tumorigenicity and metastatic spread, which are characteristics to basal-like PDA tumors.

A study of a genetically engineered mouse model of PDA places the YAP pathway downstream of the mutant KRAS signaling[32]. Similarly, our results suggest that concordant activations of TEAD2 and KRAS pathways appear in basal-like subtype of PDA. Although the cause-effect relationship between these pathways is yet to be clarified, suppressing the mutant KRAS target genes by impairing TEAD2 function suggests that they are complementary, rather than mutually independent, in supporting the development of the basal-like subtype PDA.

While this study is not the first one implicating a connection between TEAD2 and a basal-like PDA subtype, whether TEAD2 is simply a biomarker or plays a functional role in basal-like subtype PDA has not been thoroughly examined. For example, the relapse of PDA when the mutant KRAS expression is suppressed requires TEAD2 and, importantly, such relapsed PDAs have gene expressions similar to that of the basal-like subtype being activated[33]. Classifying human PDA cell lines according to their grade and degree of differentiation based on gene expression profiles shows that the higher the grade/undifferentiated PDA cell lines are, the higher their TEAD2 expression is[34]. Furthermore, the nuclear localization of TEAD2 is associated with histologically undifferentiated pattern and a poor prognosis, indicating the importance of TEAD2 in basal-like PDA[35]. It is noteworthy that different from TP63, our data indicate that TEAD2 has a vital role in establishing the *de novo* identity of tumor cells by implementing endothelial lineage-like programs in basal-like PDA cells.

In summary, our findings suggest that the acquisition of TEAD2-dependent enhancer activity controls the trajectory of the PDA subtype by epigenetic regulation. Since we implicate TEAD2-CD109-JAK/STATs as a functional axis in basal-like-differentiated PDA cells, although detailed mechanism on how CD109 activates JAK/STAT signaling needs further exploration, targeting this pathway may represent a strategy to convert basal-like PDA cells to classical cells to overcome the therapeutic insensitivity or acquired resistance occurred in current therapeutic regimens.

Supplementary Material

Refer to Web version on PubMed Central for supplementary material.

GRANT SUPPORT

This study was supported by grants from the National Research Foundation of Korea (2021R1A2C4001420 and 2020M3F7A1094089) to J-.S.R.. Brain Korea 21 FOUR Program to J-.S.R., H-.B.Y. and H-.R.K.. M-.Y.K is supported by the Basic Science Research Program through the NRF of Korea (NRF-2019R1A2C2007207 and NRF-2020M3E5E2037170) and by KAIST Grand Challenge 30 Project (KC30, N11210111) from KAIST and the Ministry of Science and ICT. K.M. is supported by grants from Japan Society for the Promotion of Science KAKENHI, Daiichi Sankyo Foundation of Life Science and SGH foundation. D.A.T is a distinguished scholar and Director of the Lustgarten Foundation-designated Laboratory of Pancreatic Cancer Research, and also supported by the Cancer Center Support Grant 5P30CA045508 (and the Animal Shared Resource for this study), the Cold Spring Harbor Laboratory Association, and the National Institutes of Health (U01CA210240, R01CA229699, U01CA224013, 1R01CA188134, and 1R01CA190092).

AVAILABILITY OF DATA AND MATERIALS

Further information and requests for resources and reagents should be directed to and will be fulfilled by the lead contact, Jae-Seok Roe (jroe@yonsei.ac.kr). The ChIP-seq, ATAC-seq, and RNA-seq data reported in this study are available in the Gene Expression Omnibus (GEO) database under GSE202534.

ABBREVIATIONS

ChIP	Chromatin immunoprecipitation
GO	gene ontology
NGS	next-generation sequencing
PDA	pancreatic ductal adenocarcinoma
seq	Sequencing
shRNA	small hairpin RNA
TF	transcription factor
VM	vascular mimicry

REFERENCE

1. Qian Y, Gong Y, Fan Z, et al. Molecular alterations and targeted therapy in pancreatic ductal adenocarcinoma. J Hematol Oncol 2020;13:130. [PubMed: 33008426]
2. Bailey P, Chang DK, Nones K, et al. Genomic analyses identify molecular subtypes of pancreatic cancer. Nature 2016;531:47–52. [PubMed: 26909576]
3. Collisson EA, Sadanandam A, Olson P, et al. Subtypes of pancreatic ductal adenocarcinoma and their differing responses to therapy. Nat Med 2011;17:500–3. [PubMed: 21460848]
4. Moffitt RA, Marayati R, Flate EL, et al. Virtual microdissection identifies distinct tumor- and stroma-specific subtypes of pancreatic ductal adenocarcinoma. Nat Genet 2015;47:1168–78. [PubMed: 26343385]
5. Chan-Seng-Yue M, Kim JC, Wilson GW, et al. Transcription phenotypes of pancreatic cancer are driven by genomic events during tumor evolution. Nat Genet 2020;52:231–240. [PubMed: 31932696]
6. Aung KL, Fischer SE, Denroche RE, et al. Genomics-Driven Precision Medicine for Advanced Pancreatic Cancer: Early Results from the COMPASS Trial. Clin Cancer Res 2018;24:1344–1354. [PubMed: 29288237]

7. Somerville TDD, Xu Y, Miyabayashi K, et al. TP63-Mediated Enhancer Reprogramming Drives the Squamous Subtype of Pancreatic Ductal Adenocarcinoma. Cell Rep 2018;25:1741–1755 e7. [PubMed: 30428345]
8. Adams CR, Htwe HH, Marsh T, et al. Transcriptional control of subtype switching ensures adaptation and growth of pancreatic cancer. Elife 2019;8.
9. Morrisey EE, Tang Z, Sigrist K, et al. GATA6 regulates HNF4 and is required for differentiation of visceral endoderm in the mouse embryo. Genes Dev 1998;12:3579–90. [PubMed: 9832509]
10. Brunton H, Caligiuri G, Cunningham R, et al. HNF4A and GATA6 Loss Reveals Therapeutically Actionable Subtypes in Pancreatic Cancer. Cell Rep 2020;31:107625. [PubMed: 32402285]
11. Miyabayashi K, Baker LA, Deschenes A, et al. Intraductal Transplantation Models of Human Pancreatic Ductal Adenocarcinoma Reveal Progressive Transition of Molecular Subtypes. Cancer Discov 2020;10:1566–1589. [PubMed: 32703770]
12. Andricovich J, Perkail S, Kai Y, et al. Loss of KDM6A Activates Super-Enhancers to Induce Gender-Specific Squamous-like Pancreatic Cancer and Confers Sensitivity to BET Inhibitors. Cancer Cell 2018;33:512–526 e8. [PubMed: 29533787]
13. Steele CW, Karim SA, Leach JDG, et al. CXCR2 Inhibition Profoundly Suppresses Metastases and Augments Immunotherapy in Pancreatic Ductal Adenocarcinoma. Cancer Cell 2016;29:832–845. [PubMed: 27265504]
14. Raghavan S, Winter PS, Navia AW, et al. Microenvironment drives cell state, plasticity, and drug response in pancreatic cancer. Cell 2021;184:6119–6137 e26. [PubMed: 34890551]
15. Kang Y, Pantel K. Tumor cell dissemination: emerging biological insights from animal models and cancer patients. Cancer Cell 2013;23:573–81. [PubMed: 23680145]
16. Hingorani SR, Wang L, Multani AS, et al. Trp53R172H and KrasG12D cooperate to promote chromosomal instability and widely metastatic pancreatic ductal adenocarcinoma in mice. Cancer Cell 2005;7:469–83. [PubMed: 15894267]
17. Aiello NM, Maddipati R, Norgard RJ, et al. EMT Subtype Influences Epithelial Plasticity and Mode of Cell Migration. Dev Cell 2018;45:681–695 e4. [PubMed: 29920274]
18. Yachida S, Iacobuzio-Donahue CA. The pathology and genetics of metastatic pancreatic cancer. Arch Pathol Lab Med 2009;133:413–22. [PubMed: 19260747]
19. McLean CY, Bristor D, Hiller M, et al. GREAT improves functional interpretation of cis-regulatory regions. Nat Biotechnol 2010;28:495–501. [PubMed: 20436461]
20. Wagenblast E, Soto M, Gutierrez-Angel S, et al. A model of breast cancer heterogeneity reveals vascular mimicry as a driver of metastasis. Nature 2015;520:358–62. [PubMed: 25855289]
21. Liu-Chittenden Y, Huang B, Shim JS, et al. Genetic and pharmacological disruption of the TEAD-YAP complex suppresses the oncogenic activity of YAP. Genes Dev 2012;26:1300–5. [PubMed: 22677547]
22. Connor AA, Denroche RE, Jang GH, et al. Integration of Genomic and Transcriptional Features in Pancreatic Cancer Reveals Increased Cell Cycle Progression in Metastases. Cancer Cell 2019;35:267–282 e7. [PubMed: 30686769]
23. Mueller S, Engleitner T, Maresch R, et al. Evolutionary routes and KRAS dosage define pancreatic cancer phenotypes. Nature 2018;554:62–68. [PubMed: 29364867]
24. Hagiwara S, Murakumo Y, Mii S, et al. Processing of CD109 by furin and its role in the regulation of TGF-beta signaling. Oncogene 2010;29:2181–91. [PubMed: 20101215]
25. Sakakura H, Mii S, Hagiwara S, et al. CD109 is a component of exosome secreted from cultured cells. Biochem Biophys Res Commun 2016;469:816–22. [PubMed: 26707640]
26. Chuang CH, Greenside PG, Rogers ZN, et al. Molecular definition of a metastatic lung cancer state reveals a targetable CD109-Janus kinase-Stat axis. Nat Med 2017;23:291–300. [PubMed: 28191885]
27. Heinrich PC, Behrmann I, Muller-Newen G, et al. Interleukin-6-type cytokine signalling through the gp130/Jak/STAT pathway. Biochem J 1998;334 (Pt 2):297–314. [PubMed: 9716487]
28. Yu CL, Meyer DJ, Campbell GS, et al. Enhanced DNA-binding activity of a Stat3-related protein in cells transformed by the Src oncoprotein. Science 1995;269:81–3. [PubMed: 7541555]

29. Zhong Z, Wen Z, Darnell JE Jr., Stat3: a STAT family member activated by tyrosine phosphorylation in response to epidermal growth factor and interleukin-6. Science 1994;264:95–8. [PubMed: 8140422]

30. Lee KY, Shueng PW, Chou CM, et al. Elevation of CD109 promotes metastasis and drug resistance in lung cancer via activation of EGFR-AKT-mTOR signaling. Cancer Sci 2020;111:1652–1662. [PubMed: 32133706]

31. S NK, Wilson GW, Grant RC, et al. Morphological classification of pancreatic ductal adenocarcinoma that predicts molecular subtypes and correlates with clinical outcome. Gut 2020;69:317–328. [PubMed: 31201285]

32. Zhang W, Nandakumar N, Shi Y, et al. Downstream of mutant KRAS, the transcription regulator YAP is essential for neoplastic progression to pancreatic ductal adenocarcinoma. Sci Signal 2014;7:ra42. [PubMed: 24803537]

33. Kapoor A, Yao W, Ying H, et al. Yap1 activation enables bypass of oncogenic Kras addiction in pancreatic cancer. Cell 2014;158:185–197. [PubMed: 24954535]

34. Diaferia GR, Balestrieri C, Prosperini E, et al. Dissection of transcriptional and cis-regulatory control of differentiation in human pancreatic cancer. EMBO J 2016;35:595–617. [PubMed: 26769127]

35. Drexler R, Fahy R, Kuchler M, et al. Association of subcellular localization of TEAD transcription factors with outcome and progression in pancreatic ductal adenocarcinoma. Pancreatology 2021;21:170–179. [PubMed: 33317954]

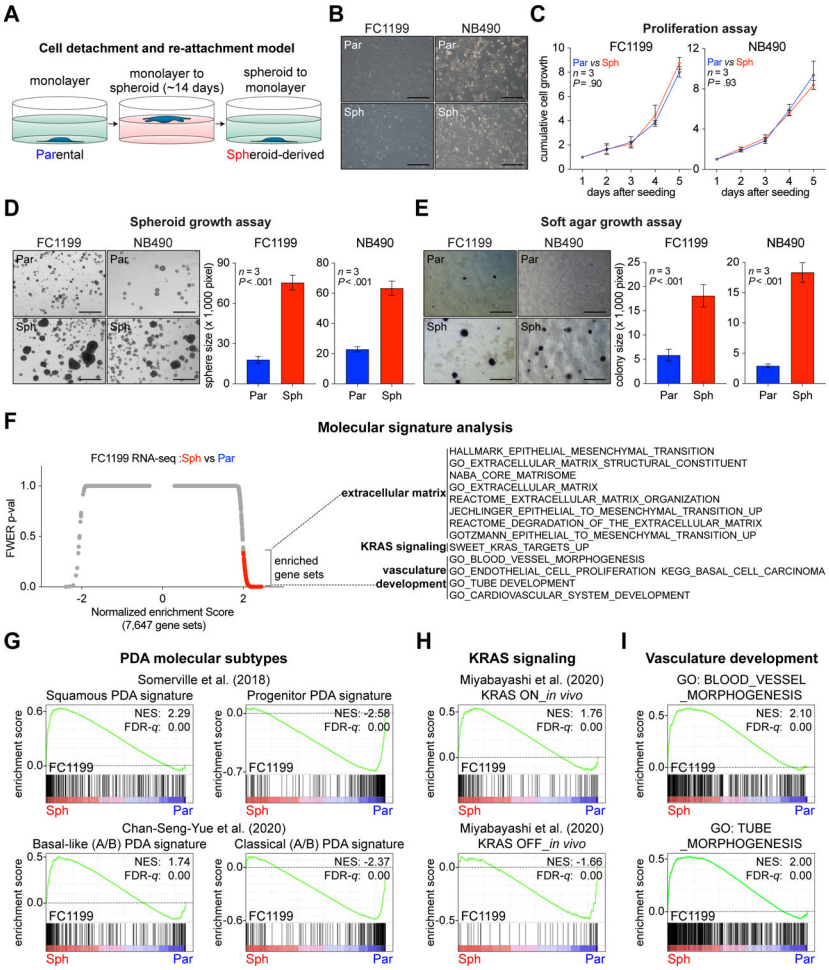

Figure 1. Cell detachment and re-attachment converts the molecular subtype of PDA cells.

(A) Schematic representation of the cell detachment and re-attachment model. (B) Morphology of Par and Sph of FC1199 and NB490 cells. (C) Proliferation of indicated cells. (D) Spheroid growth of indicated cells incubated on a low attachment plate for 3 days. (E) Soft agar assay of indicated cells. (F) Molecular signature analysis based on RNA-seq of FC1199-Par and -Sph cells. (G-I) GSEA of FC1199-Par and -Sph RNA-seq using PDA molecular subtypes signatures (G), KRAS signaling signatures (H), and vasculature development signatures (I). All *p*-values were calculated using Student's t-test, and error bars are mean +/− SEM (C-E). Normalized enrichment score (NES) and false discovery rate (FDR) q-value are shown (G-I). Scale bars: 300 μm (B) and 750 μm (D, E).

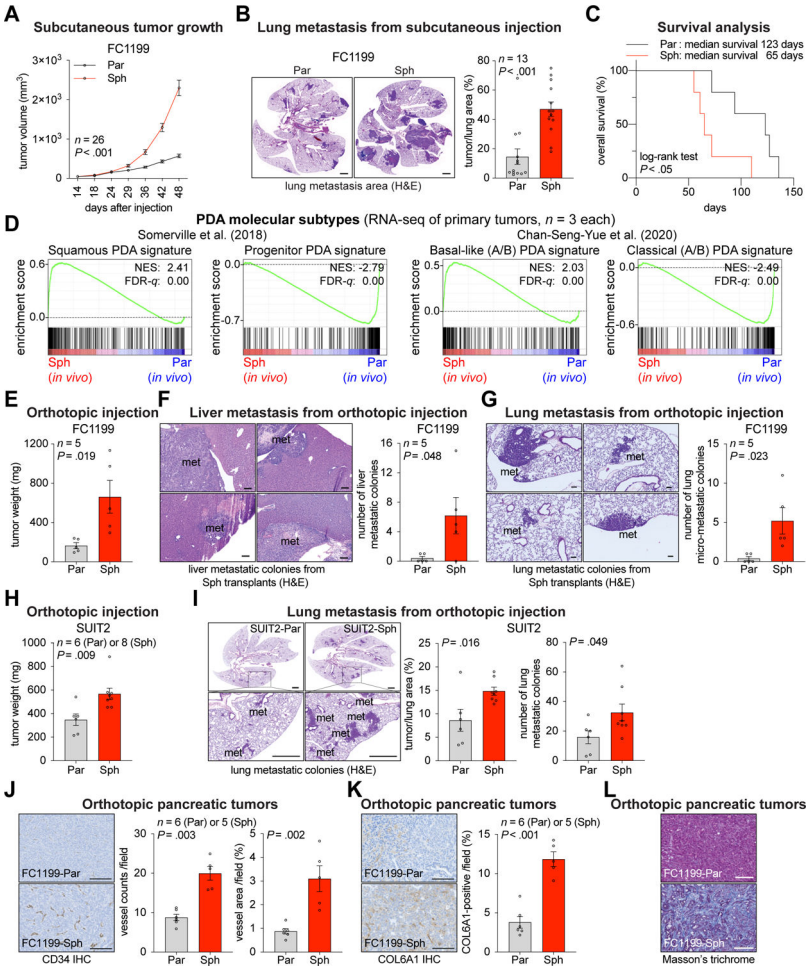

Figure 2. Basal-like subtype switching promotes PDA progression *in vivo*.

(A) Tumor growth of subcutaneously injected FC1199-Par and -Sph cells in C57BL/6J. (B) H&E staining and the percentage of of the lung area being tumor from mice subcutaneously injected with FC1199-Par and -Sph cells. (C) Kaplan-Meier survival curves of mice subcutaneously injected with FC1199-Par and -Sph cells. (D) GSEA of RNA-seq of mouse tumors derived from Par and Sph using the signature of PDA molecular subtypes. (E) Quantification of the tumor weight 4 weeks after orthotopic injection of FC1199-Par or -Sph cells in C57BL/6J mice. (F-G) H&E staining and the number of metastatic foci in the liver (F) and the lung (G) in mice orthotopically injected with FC1199-Par or -Sph cells. (H) Quantification of the tumor weight 4 weeks after orthotopic injection of SUIT2-Par or -Sph cells in nude mice. (I) H&E staining and the number of lung metastatic foci in mice orthotopically injected with SUIT2-Par or -Sph cells. (J) Representative CD34 IHC images of tumor sections (left) and quantification of the vessel counts and vessel area (%) / field (right). (K) Representative IHC images of tumor sections (left) and quantification of the COL6A1 stained area (%) / field (right). (L) Massons's trichrome histochemistry shows strong collagen fiber deposition (blue) in Sph tumors. All p-values were calculated using Student's t-test and error bars are mean +/− SEM except survival analysis which used the log-rank (Mantel–Cox) test. Scale bars: 1 mm (B, I), 100 μm (F, G, K, L) and 200 μm (J).

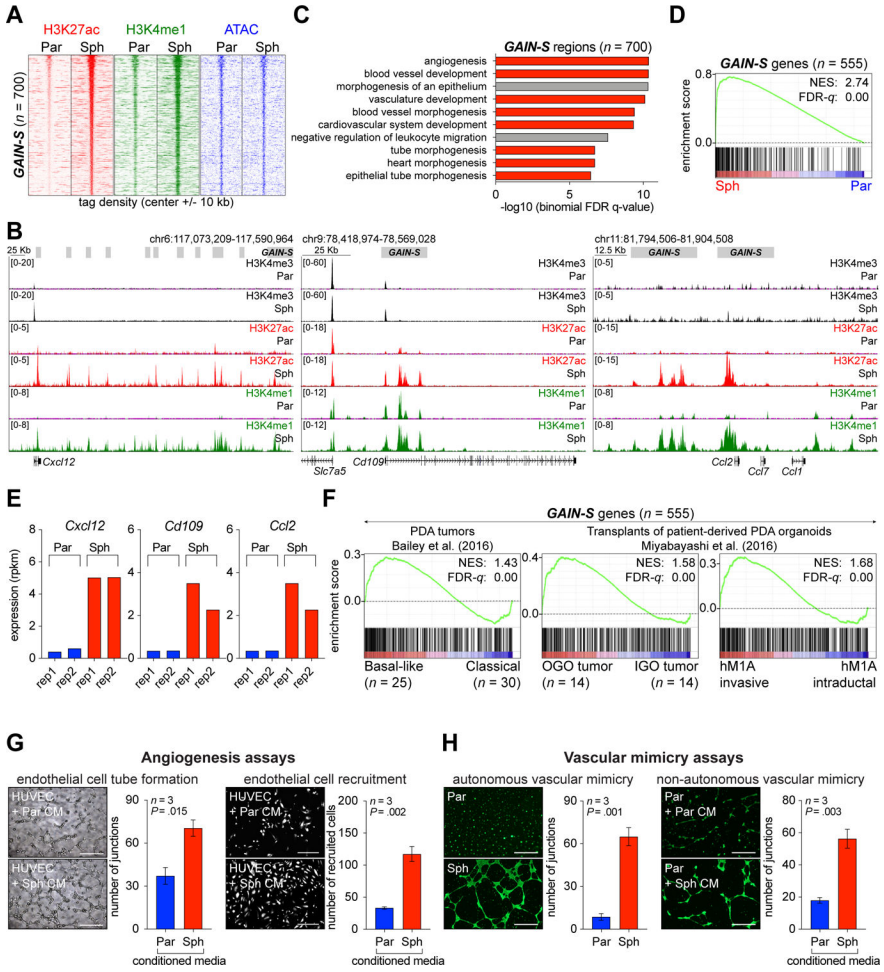

Figure 3. Basal-like subtype switching adopts endothelial-like enhancer activity in PDA cells.

(A) Density plots of H3K27ac ChIP-seq, H3K4me1 ChIP-seq, and ATAC-seq signals at *GAIN-S* regions in FC1199-Par and -Sph cells. Each row represents a single region. (B) Representative H3K4me3, H3K27ac, and H3K4me1 ChIP-seq profiles of *GAIN-S* regions, which are indicated with grey above the genome browser tracks. (C) GO analysis of genes located nearest to *GAIN-S* regions. (D) GSEA of FC1199-Par versus -Sph RNA-seq using the signature of *GAIN-S* genes. (E) Gene expression levels in human PDAs of classical and basal-like subtypes. (F) GSEA of human PDAs and human PDA organoids RNA-seq using signature of *GAIN-S* genes. (G) Tube formation and recruitment assays with HUVEC in CMs obtained from FC1199-Par and -Sph. (H) Tube formation assay of FC1199-Par or -Sph cells with serum-free media and of Par cells with Par CM or Sph CM. All *p*-values were calculated using Student's t-test and error bars are mean +/− SEM (G-H). Scale bars: 500 μm (G) and 750 μm (H).

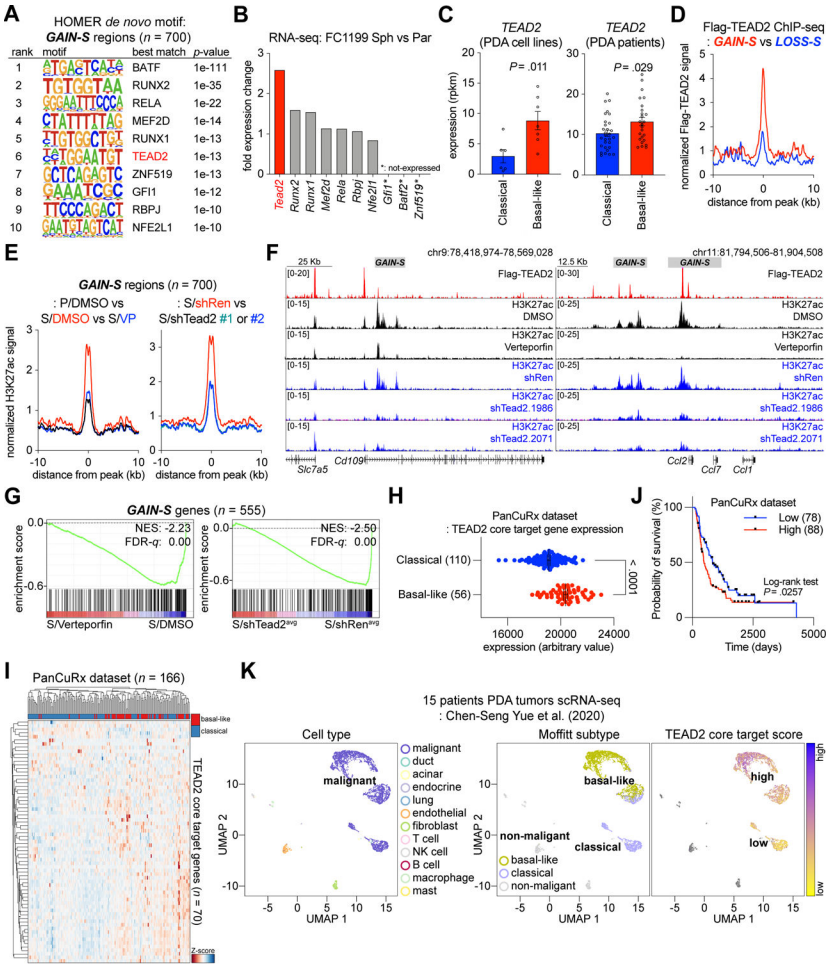

Figure 4. TEAD2 is associated with endothelial-like enhancer rewiring in basal-like PDA.

(A) The top ten *de novo* motifs enriched at *GAIN-S* regions. (B) Folds difference of the expression level of the top ten genes in (A) comparing FC1199-Sph to FC1199-Par. (C) *TEAD2* expression levels in PDA cell lines and human PDAs of classical and basal-like subtypes. (D) Metagene representations based on ChIP-Seq of Flag-TEAD2 enrichment on the *GAIN-S* or *LOSS-S* regions in Flag-TEAD2 expressing FC1199 cells. (E) Metagene representations based on ChIP-seq for H3K27ac enrichment on the *GAIN-S* regions in FC1199-Par (P)/DMSO versus Sph (S)/DMSO versus Sph/verteporfin (VP) and in FC1199-Sph/shRen versus Sph/shTead2. (F) ChIP-seq profiles of H3K27ac and Flag-Tead2 in the indicated cells. (G) GSEA of FC1199-Sph/DMSO versus VP and Sph/shRen versus shTead2 using signatures of *GAIN-S* genes. (H) Dot plots of TEAD2 core target gene expression in PDAs of classical and basal-like subtypes using PanCuRx dataset. (I) Heatmap of TEAD2 core target genes in the PanCuRx dataset. The dendrogram on top shows the clustering of PDAs. Colors on top of the heatmap indicate the subtype of PDA. (J) Survival curves of PDA patients stratified according to high or low expression of 70 TEAD2 core target genes in their tumors. (K) UMAP plots visualizing cells from scRNAseq of PDA. The sample with the greatest heterogeneity in subtype expression is shown (sample 100070). Left to right: cells are colored by cell type, distinguishing malignant cells from the stromal cell populations; malignant cells are colored by

TEAD2-dependent gene set expression score. Malignant cells that are basal-like in subtype are associated with high TEAD2-dependent gene expression.

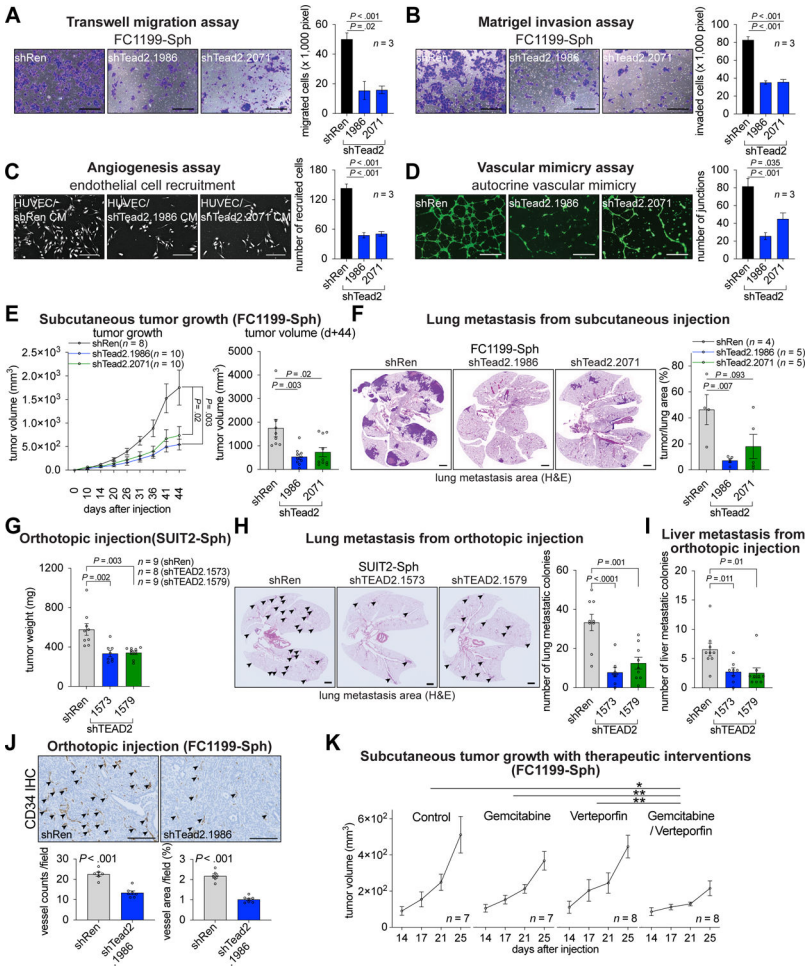

Figure 5. TEAD2 deficiency delays PDA progression and alleviates chemoresistance.

(A-B) Migration (A) and invasion (B) assay of FC1199-Sph/shRen or Sph/shTead2 cells. (C) HUVEC recruitment assay using the FC1199-Sph/shRen or Sph/shTead2 CM. (D) Tube formation assay of FC1199-Sph/shRen or Sph/shTead2. (E) Tumor growth and volume of subcutaneously injected FC1199-Sph/shRen or Sph/shTead2 cells in C57BL/6J mice. (F) H&E staining and the percentage of tumor area of lung sections from mice bearing subcutaneous tumors formed by FC1199-Sph/shRen or Sph/shTead2 cells. (G) Tumor weight after orthotopic injection of SUIT2-Sph cells expressing indicated shRNAs in NSG mice. (H-I) The number of metastatic colonies in the lung (H) and liver (I) from mice orthotopically injected with shRNA-expressing SUIT2-Sph cells. (J) Representative mCD34 IHC images of tumor sections and quantification of the vessel counts and vessel area (%) / field in Figure S5G. (K) Tumor volume curves of subcutaneous tumors by FC1199-Sph cells treated with vehicle, gemcitabine, verteporfin, or gemcitabine/verteporfin. All *p*-values were calculated using Student's t-test and error bars are mean +/− SEM. Scale bars: 300 μm (A, B), 500 μm (C), 750 μm (D), 1 mm (F, H) and 200 μm (J).

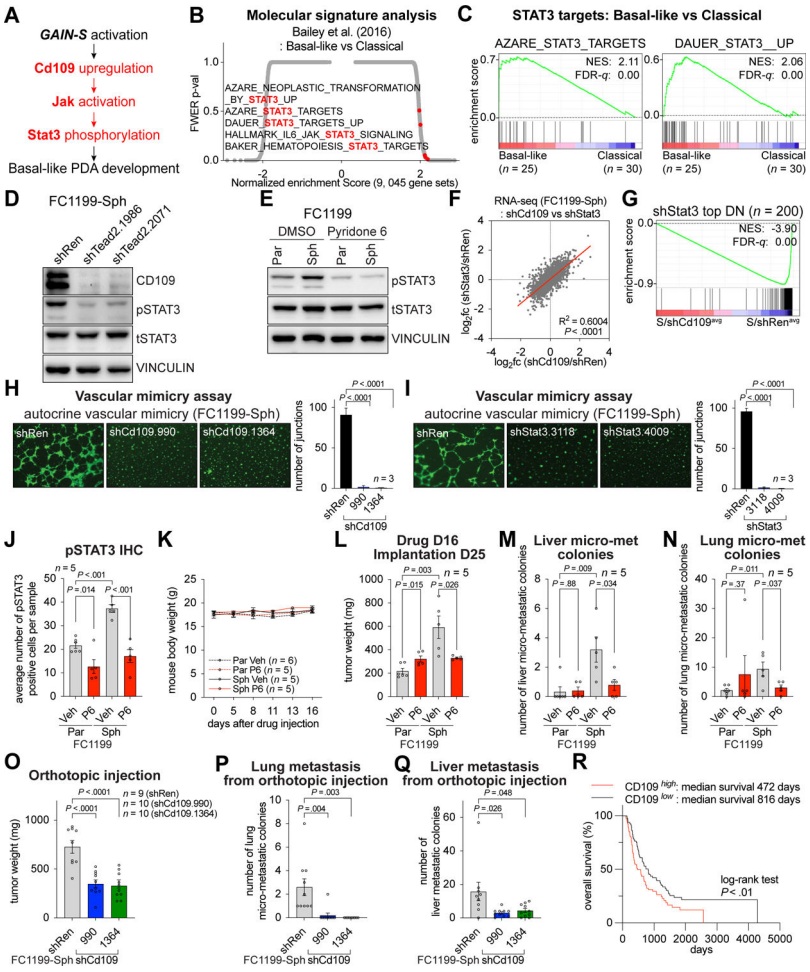

Figure 6. CD109 potentiates JAK-STAT signaling and maintains PDA progression.

(A) Schematic diagram for the TEAD2-mediated JAK-STAT activation model. (B) Molecular signature analysis based on RNA-seq of basal-like and classical subtypes of human PDA. (C) GSEA of human PDA RNA-seq data using signatures of STAT3 target genes. (D-E) Western blot analysis of FC1199-Sph/shRen or Sph/shTead2 (D) and FC1199-Par and -Sph cells treated with DMSO or P6 (E). (F) Scatter plot of Sph/shCd109 and Sph/shStat3 RNA-seq data. (G) GSEA of Sph/shRen versus Sph/shCd109 RNA-seq data using the signatures of shStat3 top DN genes. (H-I) Tube formation assay of Sph/shRen or Sph/shCd109 cells (H) and Sph/shStat3 cells (I). (J-N) The number of pSTAT3 positive cells per field resulting from IHC staining of pSTAT3 in tumors (J), the body weight (K), tumor weight (L), and the number of micro-metastatic colonies in the liver (M) and lung (N) in C57BL/6J mice orthotopically injected with Par or Sph cells and intraperitoneally injected with P6 at 0.5mg/kg every day for 16 days. (O-Q) Quantification of the tumor weight (O) and metastatic colonies in the lung (P) and liver (Q) after orthotopic injection of Sph/shRen or Sph/shCd109 cells in C57BL/6J mice. In shCd109#1364, a mouse with nine colonies metastasizing to the lung considered an outlier and excluded. (R) Survival curves of patients stratified according to high or low expression of CD109 in their PDA. All *p*-values were calculated using Student's t-test in (J-Q). Scale bar, 750 μm (H-I).

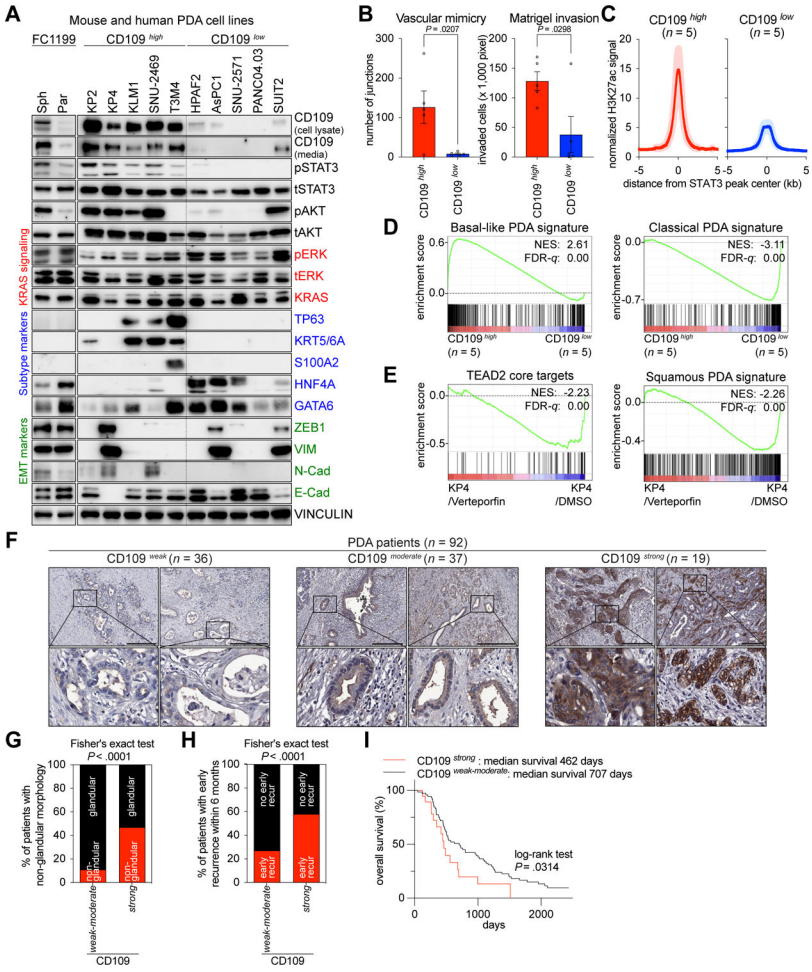

Figure 7. JAK-STAT3 is activated in human PDA cells with CD109 upregulation.

(A) Western blot analysis of indicated proteins from FC1199-Par/Sph pair (left) and 10 human PDA cell lines (right). (B) Tube formation and invasion assay in CD109^{high} and CD109^{low} human PDA cells. (C) Metagene representations based on ChIP-seq for H3K27ac enrichment on the center of STAT3 peaks. (D) GSEA of RNA-seq data using signatures of human PDA subtype. (E) GSEA of KP4/verteporfin versus KP4/DMSO RNA-seq data using signatures of TEAD2 core target genes and PDA squamous subtype. (F) Examples for CD109^{weak}, CD109^{moderate}, and CD109^{strong} human PDAs by IHC for CD109. (G-I) The proportion of glandular or non-glandular morphology (G), the percentage of patients with recurrence within 6 months (H), and overall survival (I). Scale bar, 200 μm (F).